Science of the Total Environment 716 (2020) 137097

Contents lists available at ScienceDirect

Science of the Total Environment

journal homepage: www.elsevier.com/locate/scitotenv

Rapid capture and SERS detection of triclosan using a silver nanoparticle core – protein satellite substrate

Bin Zhao, Tianxi Yang, Yanqi Qu, Alexander James Mills, Guodong Zhang, Lili He *

Department of Food Science, University of Massachusetts, Amherst, MA 01003, United States

HIGHLIGHTS

- A core- satellite nanostructure is constructed and confirmed by experimental measurements and theoretical calculation.
- The nanostructure acting as a 3D substrate allowes for rapid capture and highly sensitive SERS detection of triclosan (TCS).
- The excellent ability of SERS to distinguish TCS and triclocarban (TCC) suggests ultrahigh specificity of our SERS method.
- The capability and accuracy of the nanostructure for SERS detection of TCS in real environmental samples was demonstrated.

GRAPHICAL ABSTRACT

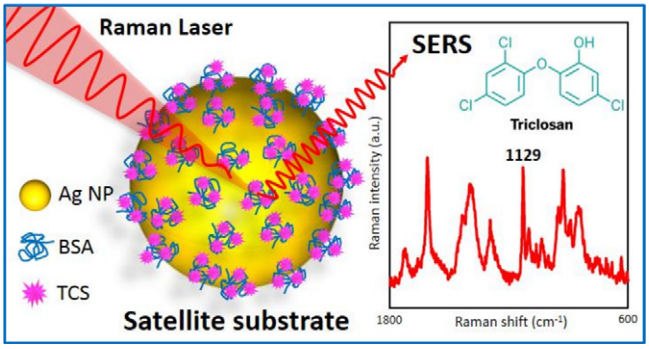

ARTICLE INFO

Article history:
Received 29 October 2019
Received in revised form 31 December 2019
Accepted 2 February 2020
Available online 3 February 2020

Editor: Yolanda Picó

Keywords:
Triclosan
Surface-enhanced Raman spectroscopy
Bovine serum albumin
Core-satellite nanostructure
Biosensor

ABSTRACT

Triclosan (TCS) is a synthetic antimicrobial compound that has been widely used in consumer products. However, increasing evidence suggests adverse effects of TCS to human health and environment, raising great public concerns. The existing methods for detecting TCS are limited to time-consuming and complicated procedure. Here, we developed a rapid method for capture and detection of TCS using surface-enhanced Raman spectroscopy (SERS) based on a silver nanoparticle (Ag NP) core – protein satellite nanostructure. Bovine serum albumin (BSA) assembled on Ag NPs as satellites configuration could anchor a large number of TCS molecules close to the surface of Ag NPs, producing amplified SERS signals. As low as 50 nM TCS standard was successfully detected within 30 min. We also demonstrated its capability for TCS detection in pond water. The developed SERS method holds a great promise for rapid screening of TCS in environmental and food samples.

1. Introduction

Triclosan (TCS), 2,4,4′-trichloro-2′-hydroxydiphenyl ether, is a synthetic antimicrobial compound that has been used as a common antimicrobial agent in a large number of consumer products, including antibacterial soaps, toothpastes, cosmetics, fabrics and detergents since the 1970s. However, more and more evidence suggests adverse effects of TCS to human health, including hormonal havoc, allergies and cancer, raising great public concerns (Cherednichenko et al., 2012; Allmyr et al., 2006; Bertelsen et al., 2013; Yueh et al., 2014). It has been found that TCS could increase colonic inflammation and colitis-associated colon tumorigenesis using mouse models (Yang et al.,

* Corresponding author.
E-mail address: lilihe@foodsci.umass.edu (L. He).

https://doi.org/10.1016/j.scitotenv.2020.137097
0048-9697/

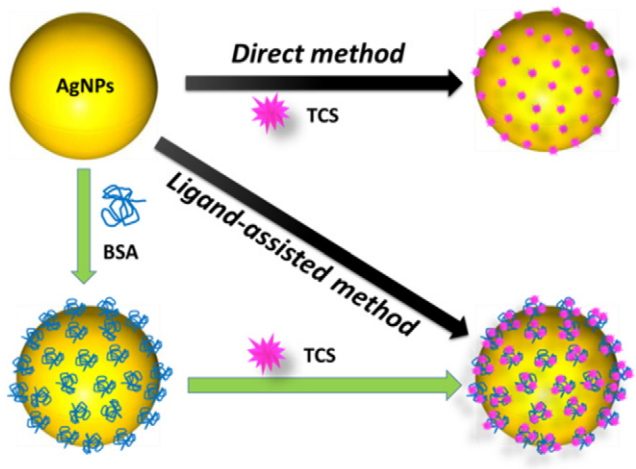

Scheme 1. Schematic illustration of SERS-based direct method and Ag NP core-protein satellite substrate-based ligand-assisted method for TCS detection. TCS = triclosan, BSA = bovine serum albumin.

2018). In addition, the widespread use of TCS in consumer products has resulted in human and environment exposure. TCS has been found in 75% of people urine samples analyzed, as well as in rivers and streams and in sewage sludge applied to agriculture (Calafat et al., 2008; Crinnion, 2010). Recent studies have demonstrated uptake and accumulation of TCS by edible plants, indicating human exposure to TCS through food crops (Mathews et al., 2014). In September 2016, FDA banned the use of TCS and 18 other chemicals in hand and body washes (U.S.F.a.D. Administration, 2016). Therefore, it is critically urgent and important to detect TCS in environmental and food samples.

Current analytical methods for TCS detection are mainly based on liquid chromatography-mass spectrometry (LC-MS) or gas chromatography–mass spectrometry (GC–MS) (Ying and Kookana, 2007; Lee et al., 2014). Analysis of samples typically includes sample preparation steps such as liquid-liquid and solid-phase extraction and derivatization of the hydroxyl group (Ying and Kookana, 2007; Lee et al., 2014). Although these methods are well-suited for their applications, they still have several disadvantages, including time-consuming, the need of high level of expertise and sophisticated operating environments. Direct and magnetic particle-based enzyme-linked immunosorbent assays (ELISA) were also employed for analysis of TCS (Shelver et al., 2007; Ahn et al., 2016). However, these methods are limited by the complicated synthesis of hapten and the use of expensive antibody. Therefore, a rapid, simple and sensitive analytical method for TCS detection is urgently needed.

Surface-enhanced Raman spectroscopy (SERS) is a variant of Raman spectroscopy that exploits nanoscale phenomena (Haynes et al., 2005). Metallic nanostructures (typically Ag and Au) can dramatically enhance the Raman cross section of molecules that are in close proximity to the metal surface due to the large electromagnetic field induced by localized surface plasmon resonance (Fleischmann et al., 1974; Albrecht and Creighton, 1977). SERS has gained much attention in recent years due to its ultra-high sensitivity and rapid analytical capability to acquire unique spectroscopic fingerprints (Lim et al., 2010; Zhao et al., 2014; Shen et al., 2014). Therefore, SERS has been emerging as a powerful analytical tool for rapid detection of, in particular, the contaminants in environmental, agricultural, food and consumer products (Halvorson and Vikesland, 2010; Zheng and He, 2014; Craig et al., 2013; Yang et al., 2016; Pang et al., 2016; Lin et al., 2008; Yan et al., 2012; Zhao et al., 2018; Dugandžić et al., 2019). However, as an emerging contaminant in environmental samples and food products, TCS, has not yet studied by SERS. Therefore, it offers a new opportunity for analysis of TCS using SERS.

Herein, we developed a novel SERS analytical platform for TCS detection in both direct and ligand-assisted manners (Scheme 1). SERS spectra of TCS was first studied by using silver nanoparticles (Ag NPs) and further used for the direct assay of TCS based on its intrinsic SERS peaks. To improve the detection sensitivity, we constructed an innovative Ag NP core - protein satellite nanostructure for ligand-assisted detection of TCS. Bovine serum albumin (BSA) protein was first assembled onto the surface of Ag NP core to form core-satellite structure. Based on ligand-molecule interaction, BSA assembled on Ag NP could anchor a large number of TCS molecules close to the surface of Ag NP, producing amplified SERS signals. The capability of the method for the differentiation of TCS and its analogue, triclocarban (TCC) was also evaluated. In addition, we applied the developed method to detect TCS spiked in pond water.

Much efforts have been made for the SERS detection of a variety of water pollutants, including organics, inorganics, and biological

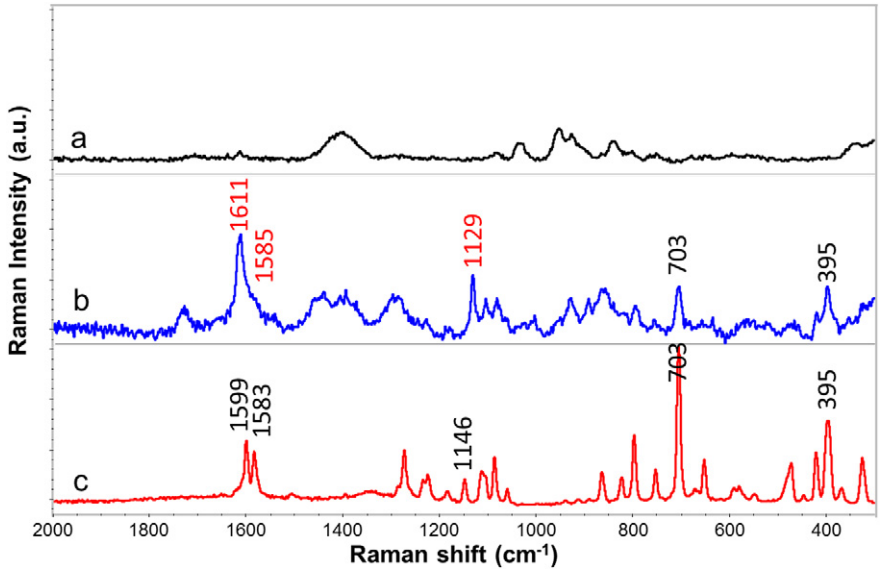

Fig. 1. Raman spectra of Ag NP background (curve a), TCS enhanced by citrate-capped Ag NP (curve b) and TCS powder (curve c).

contaminants (Li et al., 2011; Wang et al., 2014; Hao et al., 2015; Li et al., 2016; Sarfo et al., 2017; Tang et al., 2018). Our work, for the first time, reported the SERS profile of TCS enhanced by Ag NPs. The rationally designed core-satellite nanostructure has allowed for rapid capture of TCS and significantly enhanced the SERS signals, enabling rapid and highly sensitive detection of TCS. We have demonstrated the superior ability of SERS to distinguish TCS and TCC, suggesting ultrahigh specificity of our SERS method. The developed Ag NP core - protein satellite substrate also possesses excellent capability and accuracy of for SERS detection of TCS in real environmental samples.

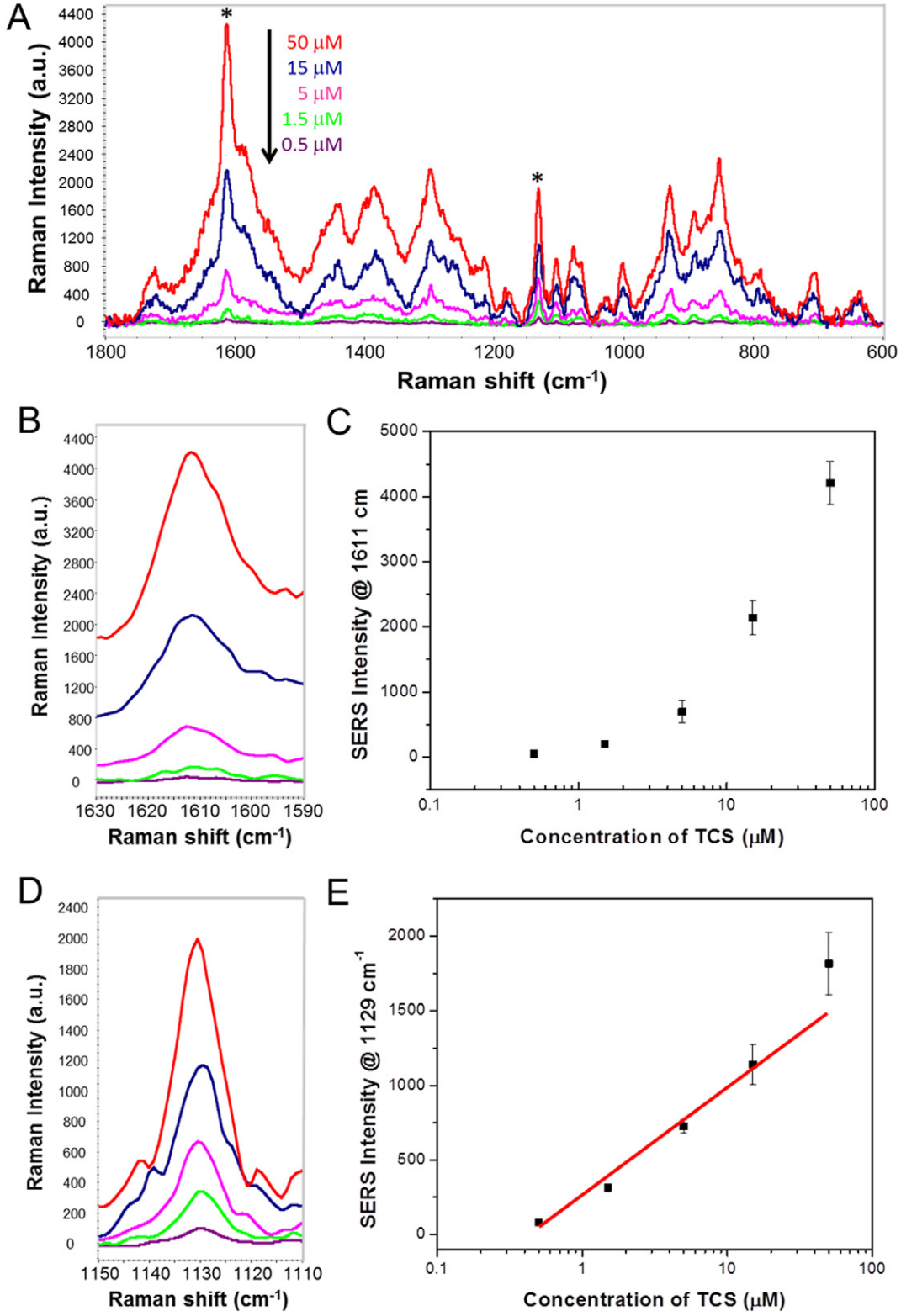

Fig. 2. (A) SERS spectra of different concentrations of TCS enhanced by Ag NP. SERS peaks at 1611 cm^{-1} and 1129 cm^{-1} indicated with asterisk were selected for quantification. (B, D) SERS spectra close-up of different concentrations of TCS at 1611 cm^{-1} and 1129 cm^{-1}, respectively. (C, E) Plot of quantitative data based on SERS peak at 1611 cm^{-1} and 1129 cm^{-1}, respectively. The tested concentration of TCS was 50, 15, 5, 1.5 and 0.5 μM, respectively.

2. Experimental

2.1. Chemicals and materials

Triclosan (TCS) and triclocarban (TCC) are purchased from Fisher Scientific (Pittsburgh, USA). Citrate-capped Ag NP (60 nm, 0.02 mg/mL) was purchased from nanoComposix (San Diego, USA). All other chemicals were purchased from Sigma-Aldrich (St. Louis, USA) unless otherwise stated. All aqueous solutions were prepared with ultrapure water (18.2 MΩ·cm) from Thermo Scientific Barnstead Smart2Pure Water Purification System.

2.2. Binding of TCS with Ag NPs

TCS stock solution (10 mM) was prepared with methanol and diluted to desired concentrations with 50% methanol solution (methanol: ultrapure water 1:1 (v/v)). The main characteristics of commercial Ag NP from the manufacturer were shown in Fig. S1 and Table S1. For SERS study of TCS, Ag NP colloid was thoroughly mixed with TCS dilution (200 μM) and ultrapure water at a volume of 2:1:1. For direct detection of TCS, a series of TCS dilutions was thoroughly mixed with water and Ag NPs at a volume of 1:1:2. The final concentration of TCS was 50, 15, 5, 1.5 and 0.5 μM. After adequate mixing and sitting at room temperature for 5 min, 2 μL of mixture was then pipetted onto a gold slide and air-dried for SERS measurement. For differentiation of TCS and TCC with direct method, TCS and TCC with the final same concentration (50 μM) was tested respectively, as mentioned above.

2.3. Ligand-assisted assay

BSA stock solution (100 μM, pH 5.5, negatively charged) was prepared and diluted to desired concentrations with ultrapure water. To verify signal amplification with BSA ligand and optimize its concentration, 5 μL of BSA solution at different concentrations was first mixed with 10 μL of Ag NP colloid and incubated at room temperature for 15 min, followed by the addition of TCS solution (5 μL). The final concentration of BSA was 0.5, 0.05, 0.005 and 0.001 μM, respectively. The final concentration of TCS was 0.5 μM. For the ligand-assisted assay, 5 μL of BSA solution with the optimal concentration (0.005 μM) was mixed with 10 μL of Ag NP colloid and incubated at room temperature

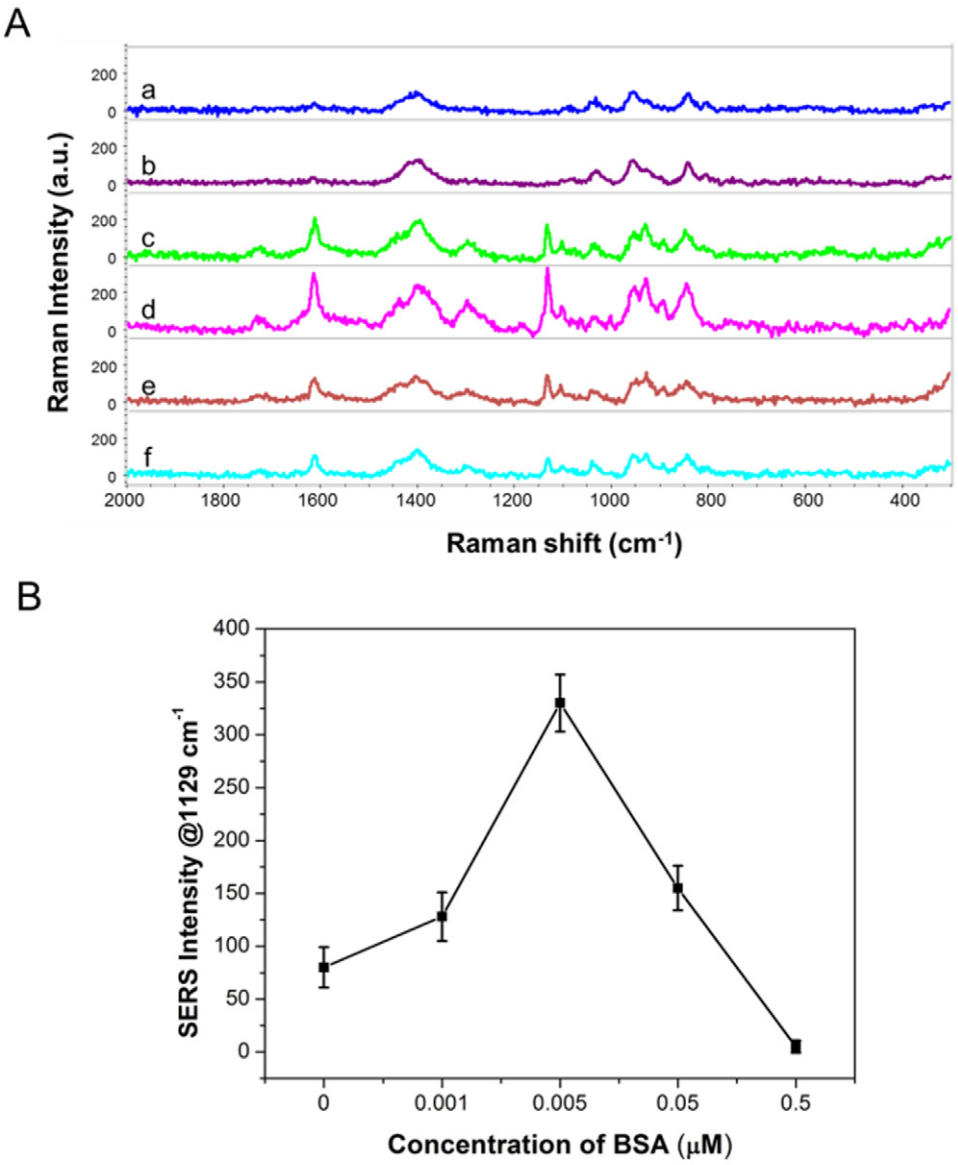

Fig. 3. (A) SERS spectra of TCS enhanced by Ag NP assembled with different concentration BSA, 0.5 (curve b), 0.05 (curve c), 0.005 (curve d) and 0.001 μM (curve e). BSA alone (curve a) and TCS alone (curve f) were set as controls. The concentration of TCS was 0.5 μM. (B) Plot of SERS intensity at 1129 cm^{-1} versus BSA concentration.

for 15 min. 5 μL of TCS standard dilutions or pond water samples spiked with TCS was then added into above mixture. Pond water was collected from UMass Campus Pond and directly used without any further treatment. After adequate mixing and sitting at room temperature for 5 min, 2 μL of mixture was pipetted onto a gold slide and air-dried for SERS measurement.

2.4. Dynamic light scattering (DLS) measurement

For DLS measurement, 50 μL of BSA solution at different concentrations was mixed with 100 μL of Ag NP colloid and incubated at room temperature for 15 min, followed by the addition of 50 μL of ultrapure water. The final concentration of BSA was 0.5, 0.05, 0.005 and 0.001 μM, respectively. Then, each sample was diluted to 800 μL with ultrapure water and analyzed using Nano-ZS Zetasizer (Malvern Instruments). All the experiments were repeated three times.

2.5. SERS measurement and data analysis

For SERS Measurement, a DXR Raman microscope (Thermo Scientific, Madison, USA) equipped with a 780 nm laser and a 20× microscope objective was used in this study. All Raman and SERS spectra were obtained with a 5.0 mW laser power and a 50 μm slit aperture for 2 s acquisition time. OMNIC 9.0 software (Thermo Scientific) was used for Raman data acquisition and analysis. Baseline correction was performed for all the obtain Raman/SERS spectra by using Automatic Baseline Correction tool in the OMNIC software. For each sample, five spots were selected randomly and scanned. The mean and standard deviation were analyzed. All the experiments were repeated three times. The 3D principal component analysis (PCA) was conducted using TQ Analyst software (Thermo Scientific) to compare the statistical difference between TCS and TCC.

3. Results and discussion

3.1. SERS spectra of TCS and direct SERS assay

Fig. 1 shows the Raman spectra of Ag NP background, TCS enhanced by citrate-capped Ag NP and TCS powder. Ag NP itself (Fig. 1-a) exhibited noise signals in the range of 800–1100 and 1350–1500 cm^{-1}. SERS spectra of TCS enhanced by citrate-capped Ag NPs were shown in Fig. 1-b. Compared to the intrinsic Raman spectra (Fig. 1-c), characteristic SERS peaks at 703 and 395 cm^{-1} are the same while new peaks at 1611, 1585 and 1129 cm^{-1} were observed. The strong peaks at 1611, 1129 and 703 cm^{-1} are assigned to aromatic ring C═C stretching vibrations, C—O—C asymmetric stretching vibrations and C—Cl stretching vibrations, respectively.

Table 1
DLS measurement of Ag NP - BSA complex.

BSA concentration (μM)	Size (nm, mean ± SD (n = 3))
0	90.4 ± 1.3
0.001	89.5 ± 2.1
0.005	96.4 ± 1.5
0.05	115.9 ± 5.0
0.5	124.9 ± 4.7

Direct mixing Ag NPs and various concentrations of TCS ranging from 50 μM to 0.5 μM were tested. As shown in Fig. 2A, SERS peaks were clearly observed, and their overall intensity gradually decreased with decreasing concentration of TCS. SERS peaks at 1611 cm^{-1} and 1129 cm^{-1} were selected for TCS quantification study (Fig. 2B–E). The intensity of SERS peaks at 1611 cm^{-1} drastically decreased as TCS concentration decreased from 50 μM to 0.5 μM. However, the intensity decrease did not show a good linear relationship with the concentration change and large variations were found for high levels of TCS. By carefully analyzing the peaks in the range of 1580–1650 (Fig. S2), it is found that this is probably attributed to the interference from the peaks at 1615 and 1606 cm^{-1}. In contrast, SERS peaks of TCS at 1129 cm^{-1} show a good linear relationship between SERS intensity and TCS concentration and variations were small. The fitting equation is $y = 722.948 \log x - 675.730$, with an R square ($R^2$) = 0.926. In contrast, there was no signal observed at 1129 cm^{-1} for Ag NP itself in the absence of TCS (blank control, Fig. 1-a). Based on its good quantitative ability, SERS peak at 1129 cm^{-1} was selected for TCS quantification in the following study.

3.2. Construction and characterization of a Ag NP core - protein satellite substrate

To further improve the sensitivity, we used BSA as a ligand binding molecule to construct a Ag NP core - protein satellite substrate for the development of ligand-assisted SERS assay for TCS detection (Scheme 1). BSA first anchored onto the surface of Ag NP surface and then acted as a bridge for TCS binding. BSA was chosen as the

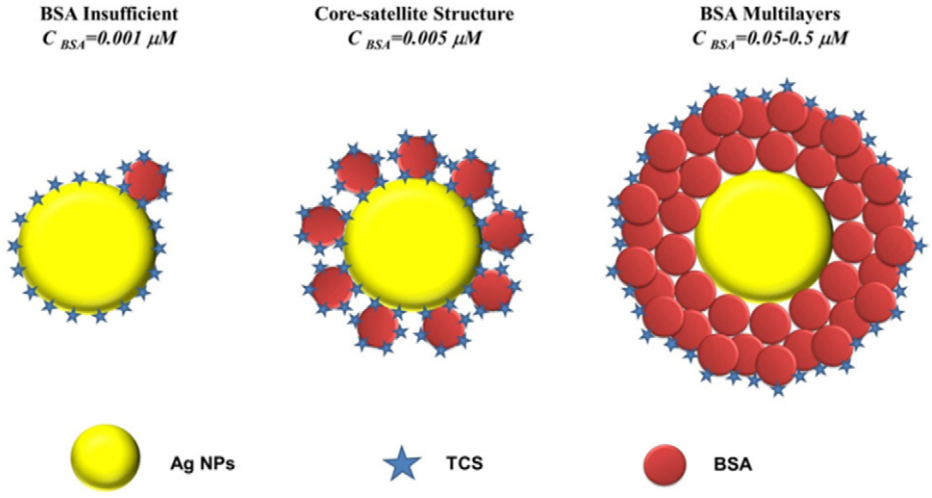

Scheme 2. Schematic illustration of different Ag NP-BSA structures (not drawn to scale) produced with different BSA concentrations, 0.001 μM (left, BSA insufficient), 0.005 μM (middle, core-satellite structure), 0.05 and 0.5 μM (right, BSA multilayers). The bound TCS molecules are also shown.

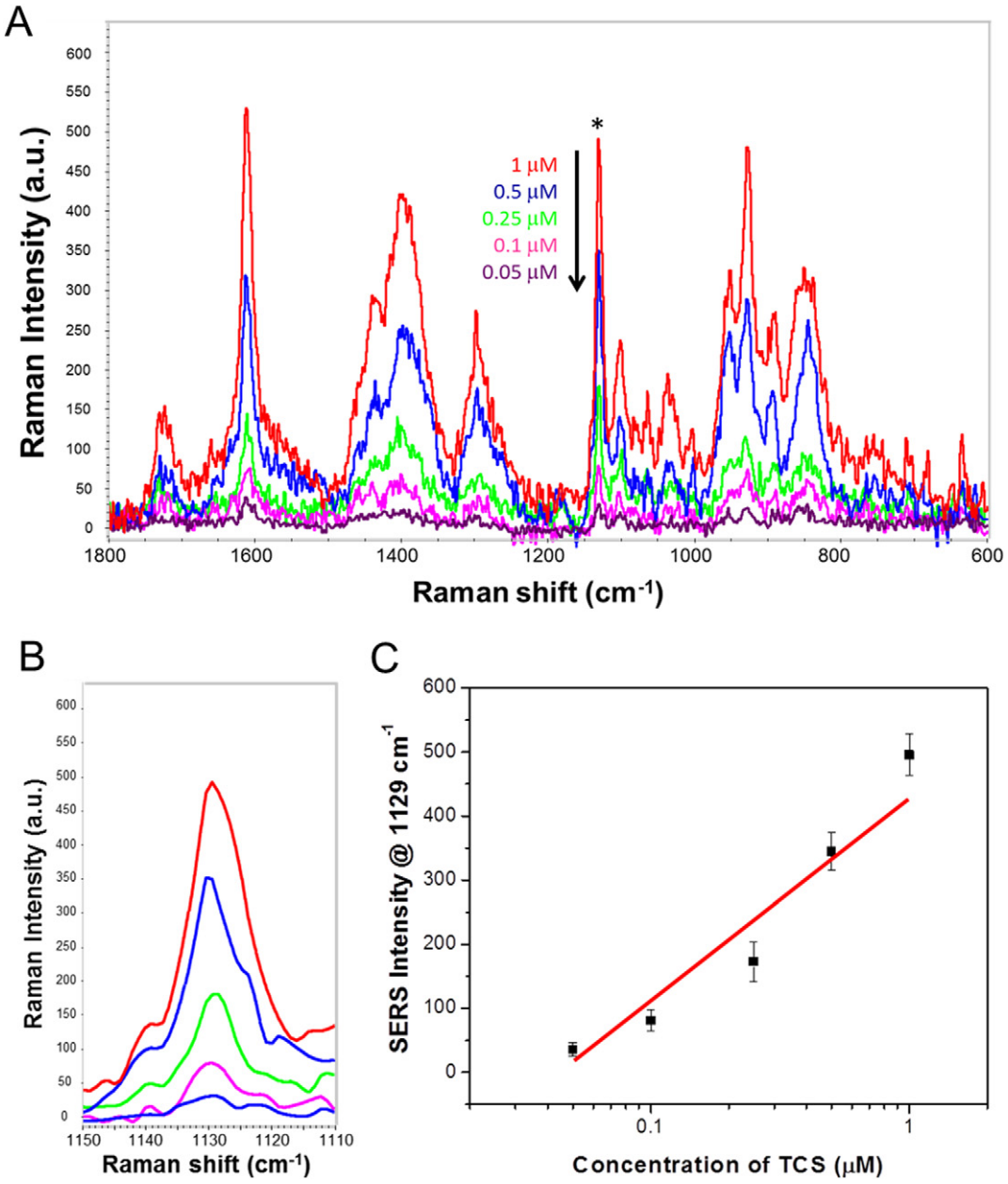

Fig. 4. (A) SERS spectra of different concentrations of TCS with BSA-assisted method. SERS peaks at 1129 cm^{-1} indicated with asterisk was used for quantification. (B) SERS spectra close-up of different concentrations of TCS at 1129 cm^{-1}. (C) Plot of quantitative data based on SERS peak at 1129 cm^{-1}.

ligand because it was reported to have a strong binding ability with TCS through mainly hydrophobic interaction (Chen et al., 2012). In addition, there was negligible SERS signals for BSA itself so that it did not produce interfering background signals (Fig. 3A-a). The use of core-satellite structure rather than monolayer or multilayer structure is to bring down the BSA interacted TCS close to the Ag NP surface. It is known that SERS effect strongly depends on the distance of analyte to the substrate surface. SERS intensity distance dependence is described in Eq. (1):

$$I_{SERS} = [(a + r)/a]^{-10} \quad (1)$$

where a is the average size of the enhancing metallic feature and r the distance between the analyte and the metallic surface (Stiles et al., 2008). The closer the analyte to the surface, the larger the enhancement factor is.

Therefore, optimizing the concentration of BSA was critical to construct the core – satellite structure and maximize the sensitivity. In experiments, we chose four concentrations of BSA ranged from 0.001 to 0.5 μM for the capture and detection of 0.5 μM of TCS. Fig. 3B showed enhanced TCS signals when 0.001 to 0.5 μM BSA was used compared to the direct method without BSA. The highest signals of TCS were achieved when 0.005 μM BSA was used, while the 0.5 μM BSA resulted in even lower signals than the control (without BSA). This result can be explained by the different Ag NP-BSA structure produced with different BSA concentrations (Scheme 2) and supported by the different hydrodynamic diameters of Ag NP-BSA complexes (Table 1). The hydrodynamic diameter of citrate-capped Ag NPs was 90 nm, that is, larger than that measured by transmission electron microscopy (~60 nm, Fig. S1) from the company. This is probably ascribed to that DLS measures the hydrodynamic diameter of the particle including the coating and solvation layers.

We further confirmed core-satellite structure with theoretical calculation. The molar concentration of Ag NP could be calculated based on Beer-Lambert law:

$$C_{Ag} = A/(\varepsilon \times d_0) \quad (2)$$

According to a previous study (Paramelle et al., 2014), the extinction coefficient for 60 nm citrate-capped Ag NP, ε, is 739 M^{-1} $cm^{-1} \times 10^8$. d_0 is 1 cm. A is determined to be 2.1849 by UV–Vis spectra. Therefore, the calculated molar concentration of 60 nm citrate-capped Ag NP, C_{Ag} is 0.03 nM.

The number of BSA on Ag NP surface in a single layer could be estimated with Eq. (3) (Chaudhary et al., 2014):

$$N = 4\pi (R + h/2)^2/A_1 \quad (3)$$

where R is the radius of the nanoparticle, h is the height of the docked protein for a particular conformation, $A_1 = \pi \times a \times b$ is the cross section of the BSA for a specific orientation. In our case, R = 30. h and A_1 varies depending upon docking orientations. BSA has a dimension of 9 nm × 9 nm × 4 nm. When BSA molecules adsorb on Ag NP surface with perpendicular orientation, the number of BSA on Ag NP surface is maximum, defined as N_{max}. According to Eq. (3), $N_{max} = 4\pi (30 + 9/2)^2/(\pi \times 4.5 \times 2) = 529$. When BSA molecules adsorb on Ag NP surface with parallel orientation, the number of BSA on Ag NP surface is minimum, defined as N_{min}. Similarly, according to Eq. (3), $N_{min} = 4\pi (30 + 4/2)^2/(\pi \times 4.5 \times 4.5) = 202$.

In our study, the number of Ag NPs, n_{Ag}, is 3×10^{-16} mol (0.03 nM × 10 μL). Therefore, the total number of BSA on all Ag NP surface to form a single layer is theoretically ranging from 6.06×10^{-14} mol ($N_{Total\ min} = N_{min} \times n_{Ag}$) to 1.58×10^{-13} mol ($N_{Total\ max} = N_{max} \times n_{Ag}$). When the concentration of BSA is 0.005 μM (optimal concentration), the number of BSA is 1×10^{-13} mol, which is exactly between $N_{Total\ min}$ and $N_{Total\ max}$. Presumably, the monolayer of BSA is formed on the surface of Ag NPs. This estimation is in a good agreement with the DLS diameter analysis of Ag-BSA structure produced by 0.005 μM BSA, where the gap between BSA molecules allowed the TCS to be the closest (0 to 3 nm) to the Ag NP surfaces. Consequently, Ag NP core-BSA protein satellite structure formed leading to the enhanced SERS signal upon the binding of TCS. For a higher concentration of BSA (0.05 or 0.5 μM), Ag NPs are likely to be covered by BSA multilayer. This was confirmed by DLS measurement showing the Ag NP-BSA structure displayed an increase of 13/17 nm in radius when 0. 05/0.5 μM BSA was used. In both cases, TCS molecules bound to BSA were kept far away (>10 nm) from Ag NP surface, where SERS enhancements were not favorable.

3.3. Ligand-assisted assay based on Ag NP core - protein satellite substrate

With the fabricated core-satellite substrate, we challenged the method with lower concentrations (1 μM to 0.05 μM) of TCS (Fig. 4A). As aforementioned, SERS peak at 1129 cm^{-1} was used for TCS quantification. Fig. 4B depicts SERS peak of TCS at 1129 cm^{-1}, which clearly shows that SERS intensity gradually reduced as TCS concentration decreased. As low as 0.05 μM TCS could be detected. This sensitivity is comparable to a previously reported electrochemical method (Yang et al., 2009). In contrast, no signal was observed at 1129 cm^{-1} for Ag NP core-BSA protein construct itself in the absence of TCS (blank control, Fig. 3A-a). Quantitative data are shown in Fig. 4C and a good linear response between TCS concentration and SERS intensity at 1129 cm^{-1} was obtained. The fitting equation is $y = 293.038 \log x + 397.870$, with an R square ($R^2$) = 0.922. The improvement of TCS detection sensitivity using ligand-assisted assay demonstrated the good capability of Ag NP core-protein structure acting as an ideal signal amplification substrate.

3.4. SERS differentiation of TCS and TCC

Given that some antibacterial consumer products may use TCS's cousin, TCC, in place of TCS (Halden and Paull, 2005). We further evaluated the capability of the developed SERS method for the differentiation of TCS and TCC with direct SERS method. Fig. 5A shows SERS spectra of TCC and its intrinsic Raman spectra, as well as SERS spectra of TCS for comparison. TCC shows a series of SERS peaks in the range from 300 to 1800 cm^{-1} which are different from its intrinsic Raman spectra due to the interaction with Ag NPs. Interestingly, TCC displays very similar SERS signature with TCS, which is attributed to the highly structural similarity between TCC and TCS. SERS peaks at 1611 and 1129 cm^{-1} were clearly observed for both TCC and TCS. Nevertheless, these two chemicals could be easily distinguished based on their distinct peaks, 677 and 632 cm^{-1} for TCC, and 703 and 395 cm^{-1} for TCS. In addition, the statistical difference was compared by principal component analysis (PCA). As shown in Fig. 5B, two discrete areas were obtained clearly, indicating that the developed SERS method was capable of differentiating TCS and TCC statistically. These results showed the excellent ability of SERS to distinguish TCS and its structural analogue, suggesting ultrahigh specificity of our SERS platform.

3.5. TCS detection in pond water

We further challenged the TCS detection in pond water with the Ag NP core - protein satellite substrate. The main characteristics of the pond water were listed in Table S2. As shown in Fig. 6, characteristic SERS peaks of TCS were clearly observed at 1611, 1129 and 703 cm^{-1}

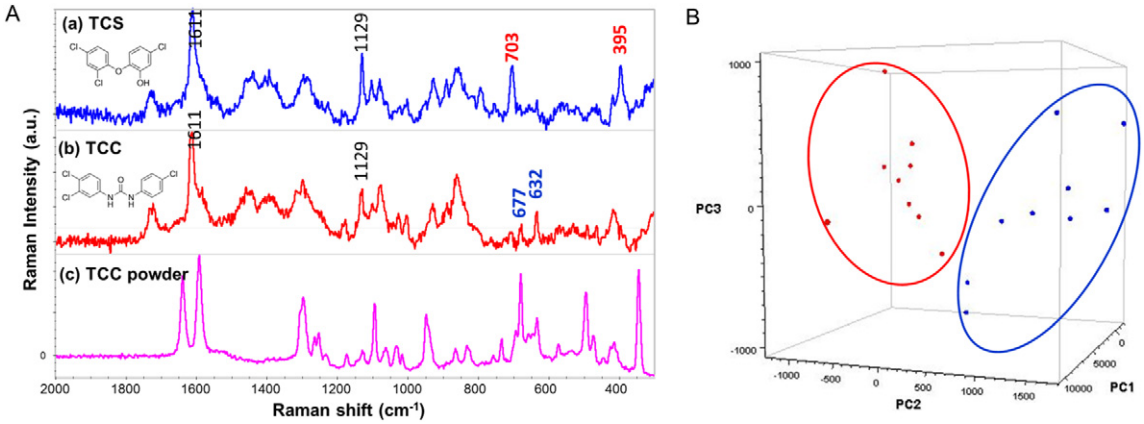

Fig. 5. (A) SERS spectra of TCS (curve a) and TCC (curve b) enhanced by Ag NP. Raman spectra of TCC powder (curve c) was as a control. (B) Principal component analysis (PCA) plot of SERS spectra of TCS (red dots) and TCC (blue dots).

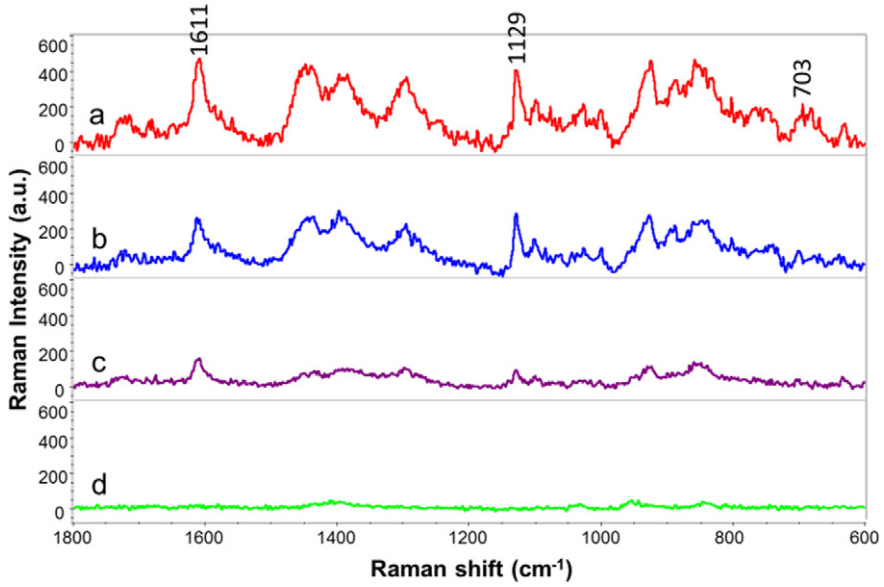

Fig. 6. SERS spectra of different concentrations of TCS in pond water with BSA-assisted assay. The concentration of TCS spiked into pond water was 1 μM (curve a), 0.4 μM (curve b) and 0.1 μM (curve c), respectively. Pond water without adding TCS was as a control (curve d).

for pond water samples spiked with different concentrations of TCS. By contrast, pond water itself displayed negligible background signals. According to the standard curve established above, the mean concentration of TCS was calculated to be 1.01, 0.38 and 0.087 μM. The recovery value (% RV) of TCS was 100.8 ± 9.5, 95.3 ± 5.7 and 87.4 ± 6.3%. In this pond water spiked test, with significant organic and inorganic interference, high sensitivity and good recovery were achieved with the developed method. Taken together, it demonstrated the capability and accuracy of the developed Ag NP core - protein satellite substrate for SERS detection of TCS in real environmental samples.

It is noteworthy that digital labeled Raman spectroscopy (DLRS) has been recently developed for the detection of TCS in antibacterial hand soaps (Han et al., 2017). Due to the fact that the peak of TCS at 701 cm^{-1} from raw Raman spectra was relatively weak, DLRS reconstructed spectra were extracted from raw Raman spectra and used for the analysis. Besides, although various metal nanostructures with complex morphology have been characterized by high aspect-ratio tips to offer superior SERS enhancement factors (Lu et al., 2007; Qian et al., 2007; Huang et al., 2011; Jiao et al., 2011; Sharma et al., 2013; Gentile et al., 2016a; Gentile et al., 2016b), these methods require complicated synthesis and precise morphology control. In comparison, our method based on the Ag NP core – BSA protein satellite SERS substrate is facile, sensitive and rapid, which can be achieved within 30 min.

4. Conclusion

In conclusion, we developed an innovative Ag NP core – BSA protein satellite substrate for detecting TCS. With the optimal structure, detection sensitivity was achieved as low as 0.05 μM (14.477 ppb). TCS and its analogue, TCC, were successfully differentiated based on their distinct SERS spectra. Moreover, TCS detection in real environmental samples, pond water, was also demonstrated. To the best of our knowledge, this is the first example of studying SERS of TCS and developing SERS-based functional nano-interface probes for TCS detection. Although the sensitivity of the developed SERS method is not as great as LC-MS or GC–MS (e.g. 50 ng/L (0.05 ppb) by LC/MS/MS in standard US EPA Method 1694), it is facile and rapid. The developed SERS platform shows great potential for rapid screening of TCS in environmental, food and consumer products, as well as biological samples.

Declaration of competing interest

The authors declare that they have no known competing financial interests or personal relationships that could have appeared to influence the work reported in this paper.

Appendix A. Supplementary data

Supplementary data to this article can be found online at https://doi.org/10.1016/j.scitotenv.2020.137097.

References

Ahn, K.C., Ranganathan, A., Bever, C.S., Hwang, S.H., Holland, E.B., Morisseau, K., Pessah, I.N., Hammock, B.D., Gee, S.J., 2016. Detection of the antimicrobial triclosan in environmental samples by immunoassay. Environ. Sci. Technol. 50, 3754–3761.
Albrecht, M.G., Creighton, J.A., 1977. Anomalously intense Raman spectra of pyridine at a silver electrode. J. Am. Chem. Soc. 99, 5215–5217.
Allmyr, M., Adolfsson-Erici, M., McLachlan, M.S., Sandborgh-Englund, G., 2006. Triclosan in plasma and milk from Swedish nursing mothers and their exposure via personal care products. Sci. Total Environ. 372, 87–93.
Bertelsen, R.J., Longnecker, M.P., Løvik, M., Calafat, A.M., Carlsen, K.H., London, S.J., Lødrup Carlsen, K.C., 2013. Triclosan exposure and allergic sensitization in Norwegian children. Allergy 68, 84–91.
Calafat, A.M., Ye, X., Wong, L.-Y., Reidy, J.A., Needham, L.L., 2008. Urinary concentrations of triclosan in the U.S. population: 2003–2004. Environ. Health Perspect. 116, 303–307.
Chaudhary, A., Gupta, A., Khan, S., Nandi, C.K., 2014. Morphological effect of gold nanoparticles on the adsorption of bovine serum albumin. Phys. Chem. Chem. Phys. 16, 20471–20482.
Chen, J., Zhou, X., Zhang, Y., Zi, Y., Qian, Y., Gao, H., Lin, S., 2012. Binding of triclosan to human serum albumin: insight into the molecular toxicity of emerging contaminant. Environ. Sci. Pollut. Res. 19, 2528–2536.
Cherednichenko, G., Zhang, R., Bannister, R.A., Timofeyev, V., Li, N., Fritsch, E.B., Feng, W., Barrientos, G.C., Schebb, N.H., Hammock, B.D., Beam, K.G., Chiamvimonvat, N., Pessah, I.N., 2012. Triclosan impairs excitation–contraction coupling and Ca2+ dynamics in striated muscle. Proc. Natl. Acad. Sci. U. S. A. 109, 14158–14163.
Craig, A.P., Franca, A.S., Irudayaraj, J., 2013. Surface-enhanced Raman spectroscopy applied to food safety. Annu. Rev. Food Sci. Technol. 4, 369–380.
Crinnion, W.J., 2010. The CDC fourth national report on human exposure to environmental chemicals: what it tells us about our toxic burden and how it assist environmental medicine physicians. Altern. Med. Rev. 15, 101–109.
Dugandžić, V., Kupfer, S., Jahn, M., Henkel, T., Weber, K., Cialla-May, D., Popp, J., 2019. A SERS-based molecular sensor for selective detection and quantification of copper (II) ions. Sensors Actuators B Chem. 279, 230–237.
Fleischmann, M., Hendra, P.J., McQuillan, A.J., 1974. Raman spectra of pyridine adsorbed at a silver electrode. Chem. Phys. Lett. 26, 163–166.
Gentile, A., Ruffino, F., D'Andrea, C., Gucciardi, P., Reitano, R., Grimaldi, M., 2016a. Solid-state synthesized nanostructured Au dendritic aggregates towards surface-enhanced Raman spectroscopy. J. Electron. Mater. 45, 2815–2825.

Gentile, A., Ruffino, F., Grimaldi, M.G., 2016b. Complex-morphology metal-based nanostructures: fabrication, characterization, and applications. Nanomaterials 6, 110.
Halden, R.U., Paull, D.H., 2005. Co-occurrence of triclocarban and triclosan in U.S. water resources. Environ. Sci. Technol. 39, 1420–1426.
Halvorson, R.A., Vikesland, P.J., 2010. Surface-enhanced Raman spectroscopy (SERS) for environmental analyses. Environ. Sci. Technol. 44, 7749–7755.
Han, X., Tan, Z., Huang, Z., Chen, X., Gong, Y., Li, Q., Xu, K., Chen, D., 2017. Nondestructive detection of triclosan in antibacterial hand soaps using digitally labelled Raman spectroscopy. Anal. Methods 9, 3720–3726.
Hao, J., Han, M.-J., Han, S., Meng, X., Su, T.-L., Wang, Q.K., 2015. SERS detection of arsenic in water: a review. JEnvS 36, 152–162.
Haynes, C.L., McFarland, A.D., Duyne, R.P.V., 2005. Surface-enhanced Raman spectroscopy. Anal. Chem. 77, 338 A–346 A.
Huang, D., Bai, X., Zheng, L., 2011. Ultrafast preparation of three-dimensional dendritic gold nanostructures in aqueous solution and their applications in catalysis and SERS. J. Phys. Chem. C 115, 14641–14647.
Jiao, Y., Ryckman, J.D., Ciesielski, P.N., Escobar, C.A., Jennings, G.K., Weiss, S.M., 2011. Patterned nanoporous gold as an effective SERS template. Nanotechnology 22, 295302.
Lee, H.-B., Kohli, J., Peart, T.E., Nguyen, N., 2014. Selected chloro and bromo derivatives of triclosan—syntheses and their occurrence in Canadian sewage and biosolid samples. Environ. Sci. Pollut. Res. 21, 314–324.
Li, D., Qu, L., Zhai, W., Xue, J., Fossey, J.S., Long, Y., 2011. Facile on-site detection of substituted aromatic pollutants in water using thin layer chromatography combined with surface-enhanced Raman spectroscopy. Environ Sci Technol 45, 4046–4052.
Li, Z., Wang, J., Li, D., 2016. Applications of Raman spectroscopy in detection of water quality. ApSRv 51, 333–357.
Lim, D.-K., Jeon, K.-S., Kim, H.M., Nam, J.-M., Suh, Y.D., 2010. Nanogap-engineerable Raman-active nanodumbbells for single-molecule detection. Nat. Mater. 9, 60–67.
Lin, M., He, L., Awika, J., Yang, L., Ledoux, D.R., Li, H., Mustapha, A., 2008. Detection of melamine in gluten, chicken feed, and processed foods using surface enhanced Raman spectroscopy and HPLC. J. Food Sci. 73, T129–T134.
Lu, G., Li, C., Shi, G., 2007. Synthesis and characterization of 3D dendritic gold nanostructures and their use as substrates for surface-enhanced Raman scattering. Chem. Mater. 19, 3433–3440.
Mathews, S., Henderson, S., Reinhold, D., 2014. Uptake and accumulation of antimicrobials, triclocarban and triclosan, by food crops in a hydroponic system. Environ. Sci. Pollut. R. 21, 6025–6033.
Pang, S., Yang, T., He, L., 2016. Review of surface enhanced Raman spectroscopic (SERS) detection of synthetic chemical pesticides. Trends Anal. Chem. 85, 73–82.
Paramelle, D., Sadovoy, A., Gorelik, S., Free, P., Hobley, J., Fernig, D.G., 2014. A rapid method to estimate the concentration of citrate capped silver nanoparticles from UV–visible light spectra. Analyst 139, 4855–4861.
Qian, L., Yan, X., Fujita, T., Inoue, A., Chen, M., 2007. Surface enhanced Raman scattering of nanoporous gold: smaller pore sizes stronger enhancements. ApPhL 90, 153120.
Sarfo, D.K., Sivanesan, A., Izake, E.L., Ayoko, G.A., 2017. Rapid detection of mercury contamination in water by surface enhanced Raman spectroscopy. RSC Adv. 7, 21567–21575.
Sharma, B., Cardinal, M.F., Kleinman, S.L., Greeneltch, N.G., Frontiera, R.R., Blaber, M.G., Schatz, G.C., Van Duyne, R.P., 2013. High-performance SERS substrates: advances and challenges. MRS Bull. 38, 615–624.
Shelver, W.L., Kamp, L.M., Church, J.L., Rubio, F.M., 2007. Measurement of triclosan in water using a magnetic particle enzyme immunoassay. J. Agr. Food Chem. 55, 3758–3763.
Shen, J., Su, J., Yan, J., Zhao, B., Wang, D., Wang, S., Li, K., Liu, M., He, Y., Mathur, S., Fan, C., Song, S., 2014. Bimetallic nano-mushrooms with DNA-mediated interior nanogaps for high-efficiency SERS signal amplification. Nano Res. 8, 731–742.
Stiles, P.L., Dieringer, J.A., Shah, N.C., Duyne, R.P.V., 2008. Surface-enhanced Raman spectroscopy. Annu. Rev. Anal. Chem. 1, 601–626.
Tang, H., Zhu, C., Meng, G., Wu, N., 2018. Surface-enhanced Raman scattering sensors for food safety and environmental monitoring. J. Electrochem. Soc. 165, B3098–B3118.
U.S.F.a.D. Administration, 2016. FDA Issues Final Rule on Safety and Effectiveness of Antibacterial Soaps.
Wang, M., De Vivo, B., Lu, W., Muniz-Miranda, M., 2014. Sensitive surface-enhanced Raman scattering (SERS) detection of nitroaromatic pollutants in water. ApSpe 68, 784–788.
Yan, J., Su, S., He, S., He, Y., Zhao, B., Wang, D., Zhang, H., Huang, Q., Song, S., Fan, C., 2012. Nano rolling-circle amplification for enhanced SERS hot spots in protein microarray analysis. Anal. Chem. 84, 9139–9145.
Yang, J., Wang, P., Zhang, X., Wu, K., 2009. Electrochemical sensor for rapid detection of triclosan using a multiwall carbon nanotube film. J. Agr. Food Chem. 57, 9403–9407.
Yang, T., Zhang, Z., Zhao, B., Hou, R.-Y., Kinchla, A., Clark, J.M., He, L., 2016. Real-time and in situ monitoring of pesticide penetration in edible leaves by surface-enhanced Raman scattering mapping. Anal. Chem. 88, 5243–5250.
Yang, H., Wang, W., Romano, K.A., Gu, M., Sanidad, K.Z., Kim, D., Yang, J., Schmidt, B., Panigrahy, D., Pei, R., Martin, D.A., Ozay, E.I., Wang, Y., Song, M., Bolling, B.W., Xiao, H., Minter, L.M., Yang, G.-Y., Liu, Z., Rey, F.E., Zhang, G., 2018. A common antimicrobial additive increases colonic inflammation and colitis-associated colon tumorigenesis in mice. Sci. Transl. Med. 10, eaan4116.
Ying, G.-G., Kookana, R.S., 2007. Triclosan in wastewaters and biosolids from Australian wastewater treatment plants. Environ. Int. 33, 199–205.
Yueh, M.-F., Taniguchi, K., Chen, S., Evans, R.M., Hammock, B.D., Karin, M., Tukey, R.H., 2014. The commonly used antimicrobial additive triclosan is a liver tumor promoter. Proc. Natl. Acad. Sci. U. S. A. 111, 17200–17205.
Zhao, B., Shen, J., Chen, S., Wang, D., Li, F., Mathur, S., Song, S., Fan, C., 2014. Gold nanostructures encoded by non-fluorescent small molecules in polyA-mediated nanogaps as universal SERS nanotags for recognizing various bioactive molecules. Chem. Sci. 5, 4460–4466.
Zhao, B., Yang, T., Zhang, Z., Hickey, M.E., He, L., 2018. A triple functional approach to simultaneously determine the type, concentration, and size of titanium dioxide particles. Environ. Sci. Technol. 52, 2863–2869.
Zheng, J., He, L., 2014. Surface-enhanced Raman spectroscopy for the chemical analysis of food. Compr. Rev. Food Sci. Food Saf. 13, 317–328.